THE JOURNAL OF PHYSICAL CHEMISTRY C
A JOURNAL OF THE AMERICAN CHEMICAL SOCIETY

pubs.acs.org/JPCC
Article

Metal–Support Interactions in Metal/Oxide and Inverse Oxide/Metal Catalysts: A Case Study Using Cu/ZnO and ZnO/Cu Model Catalysts

Chandra Chowdhury, Felix Studt, and Jelena Jelic*

Cite This: J. Phys. Chem. C 2025, 129, 5860–5867
Read Online

ABSTRACT: Metal–metal oxide interfaces comprise the most common type of "active sites" in heterogeneous catalysis. The activity of interface sites originates from geometry, namely, certain facets and their corresponding electronic structures, as well as charge transfer between the oxide support and metal particles and the binding modes that stabilize reaction intermediates. In most instances, the metal is dispersed on an oxide support in the form of particles ranging from a few nanometers to tens of nanometers in size. There are also inverse metal oxide/metal catalysts in which the oxide is dispersed on the metal surface. Herein, we employ DFT calculations using extended nanowire models representing metal particles as well as their inverse configuration. Through this, we address similarities and differences between the two types of metal–metal oxide interfaces, especially regarding their electronic properties and corresponding stabilization of important reaction intermediates. We use the well-studied Cu/ZnO catalyst and the corresponding CO/CO_2 hydrogenation to CH_3OH as an example.

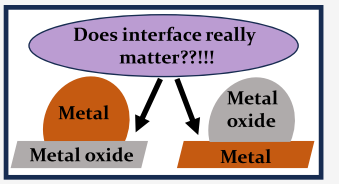

INTRODUCTION

Applications for metal nanoparticles distributed on oxide substrates range from petrochemical catalysis to energy production to environmental remediation.[1] There are several ways in which the catalytic characteristics of these nanoscale systems can be adjusted due to the structural complexity displayed by both nanoparticles and oxide phases.[2−6] Properties of the interface between the metal particles and the oxide support have been shown to have a strong correlation with the enhancement of reactivity in a number of different scenarios. For example, researchers have examined how such tuning can increase catalytic reactivity for a variety of reactions important to both renewable and conventional energy production, such as CO oxidation,[7] methanol partial oxidation,[8] CO_2 hydrogenation to methanol,[9] formic acid decomposition,[10] and the water gas shift reaction.[11] Numerous studies over the years have been aimed at enhancing our knowledge of the atomic-level structure of metal-oxide interfaces, the electronic character of the metal atoms that are directly at these interfaces, and the energetics of bonding and thermodynamic stability of these interfaces. As an alternative to using a metal-oxide catalyst, nanosized metal oxide supports, which provide a high density of defects and edge or corner surface sites, can enhance the interactions with the metal.[12] These findings have led to the development of inverse metal oxide/metal catalysts, also known as inverse catalysts, in which the metal oxide is placed onto an unsupported or supported metal surface.[13−15] Deposition of metal oxides on metal surfaces results in materials with unique chemical and electronic properties, in contrast to those of typical bulk metal oxide supports.[16,17] In the case of an inverted oxide/metal catalyst, a reactant can attach to the oxide particle's regular centers and defects, pure metal centers, and the metal-oxide interface.[18] It has been shown experimentally that the thickness of oxide adlayers on the metal substrate was demonstrated to strongly affect the electronic structures of oxide adlayers in the oxide/metal inverse catalysts.[19−21] Recently, there has been an uptick in efforts to prepare systems of this kind in forms suitable for technical applications because of the recognition that well-defined inverse oxide/metal catalysts can have distinctive features. For instance, Rodriguez et al. developed inverse catalysts and evaluated their impact on the stability of reaction intermediates.[15] Preparing powder catalysts with an inverted configuration via unique synthesis techniques or by dispersing oxide nanoparticles and metal on a substrate is necessary for a practical implementation of these inverse catalysts.[15,22] The use of inverse catalysts in industry and how the strong oxide-metal interactions (SOMIs) cause considerable perturbations in the electronic structure of both reducible and nonreducible oxides have also been extensively discussed.[23] Herein, we focus on methanol synthesis over Cu/ZnO catalysts as an example of metal/metal oxide interactions. The activity of metal/metal oxide catalysts for CO_2 hydrogenation is influenced by the composition of the oxide support, with ZnO being vividly discussed as a promoter of utmost importance, boosting the activity of the copper-based catalyst by an order of magnitude.[24] Overlayers of reduced ZnO (ZnOx) on top of the Cu particles found in Cu/ZnO catalysts have been

Received: December 31, 2024
Revised: February 11, 2025
Accepted: February 24, 2025
Published: March 12, 2025

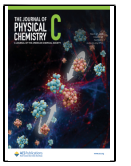

detected employing high-resolution transmission electron microscopy (HRTEM).[25,26] The catalyst's active phase thus has ZnO on copper. The reducibility of ZnO is crucial for its activity, and led to many hypotheses, from the presence of an O-vacancy enabling the relatively straightforward step of CO_2 adsorption,[27−29] to metallic Zn being incorporated into the copper surface.[30−32] Recently, several experimental reports have demonstrated the applicability of ZnO/Cu as a catalyst for CO and CO_2 hydrogenation to methanol.[33−38] Interestingly, the activity of the conventional Cu/ZnO system could be mimicked by depositing ZnO on a Cu/MgO sample that is otherwise having a rather detrimental activity compared to Cu/ZnO, highlighting the role that ZnO on the surfaces of Cu exhibits.[39]

While these studies highlight that interfacial interactions play a crucial role in both the metal-oxide and their inverse formulations, the origins of the various interactions at the atomic scale are still mostly elusive. In this study, we use density functional theory (DFT) calculations to investigate the interface of Cu and ZnO in both, the common Cu/ZnO as well as its inverse ZnO/Cu catalyst (see Figure 1). By doing so,

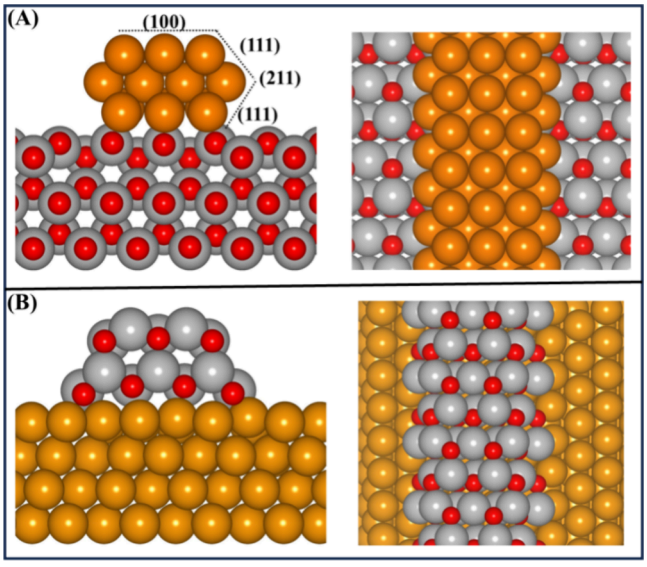

Figure 1. Schematic depiction of two catalyst arrangements for the CO/CO_2 hydrogenation processes. (A) Standard catalyst: a Cu nanowire (Cu/ZnO) is situated atop the ZnO (10−10) surface. The left panel illustrates the lateral perspective, whereas the right panel presents the top view of the model. (B) Inverse catalyst: a ZnO nanowire (ZnO/Cu) is positioned on a Cu (111) surface. The left panel depicts the lateral perspective, while the right panel presents the top view of the inverted configuration. Orange: Cu, gray: Zn, red: O.

we further shed light on the applicability of theoretical models of these interfaces and how they can be used to explain differences in binding energies for intermediates occurring in the hydrogenation of CO and CO_2 to methanol.

COMPUTATIONAL DETAILS

The Vienna ab initio simulation package (VASP)[40,41] in conjunction with the atomic simulation environment (ASE)[42] was used to carry out the density functional theory (DFT) computations. The projector augmented wave method (PAW),[43,44] the Bayesian Error Estimation Functional with van der Waals correlations (BEEF-vdW)[45] exchange-correlation functional, and a plane-wave basis set with a cutoff energy of 450 eV were employed. The choice of the BEEF-vdW functional is motivated by its ability to accurately describe surface processes associated with CO_2 hydrogenation to methanol and CO, as well as its performance in terms of adsorption energies and transition states on transition metal surfaces.[39,46−49]

Similar to the models described by Zhao et al. for Au on MgO,[50] Whittaker et al. for Au on TiO_2,[51] and Studt et al. for Cu on ZrO_2,[52] we modeled the interface between the ZnO (10−10) facet and metallic copper as Cu/ZnO using periodic slabs consisting of three-layer-thick 14 × 1 ZnO units in the x and y direction. The copper nanoparticle is modeled by a nanowire that is made up of three layers of Cu (100) aligned facets, where the bottom and top layers have 3 × 2 atoms in the x and y directions and the middle layer has 4 × 2 atoms. Importantly, this model represents the Cu/ZnO interface while being metallic, thus keeping the electronic structure of larger-sized copper particles.[53,54] Surfaces on the top and bottom of the copper nanowire show the Cu (100) orientation, while those on the sides are terminated by the Cu (111) facet. The middle Cu layer terminates at the Cu (211) facet. It follows that the Cu (100) termination is parallel to the ZnO (10−10) surface. The copper lattice is increased by 5.08% along the y-axis to make room for the nanowire of copper on the ZnO (10-10) surface. During geometry optimization, the lowest layer of ZnO was held fixed at the bulk positions while the remaining layers were allowed to relax. A 20 Å vacuum was used to separate the slabs in the z-direction. A Monkhorst−Pack k-point grid of 2 × 8 × 1 was used to sample the Brillouin zone.[55]

Our second model of the inverse ZnO/Cu catalyst used a Cu (111) surface as the support with a ZnO nanowire being supported on it. We have designed a two-layer-thick model of a ZnO nanowire, for which it has 1 × 7 ZnO units in the bottom layer and 1 × 5 ZnO units in the upper layer in the x and y directions. It is placed on top of the Cu (111) slab in such a way that the lattice mismatch is only 2.09% in the y-direction. We have taken a four-layer thick 2 × 10 large Cu slab with the bottom two layers being kept fixed during the optimization process. The k-point grid used is 8 × 2 × 1. Analyses of vibrations were performed using the finite difference method in the harmonic approximation with a resolution of 0.01 Å. The Gibbs free energies were calculated at a temperature of 500 K and 1 bar pressure.

RESULTS AND DISCUSSION

This article mainly investigates and compares the interfacial interactions between a metal/metal oxide catalyst and its inverse configuration with reaction intermediates. To enable a meaningful and precise comparison, it is important to use structurally and geometrically equivalent models to minimize deviations that could confound the results. By selecting analogous models, we can systematically investigate how the orientation and placement of the metal and metal oxide constituents affect their electronic properties and catalytic activity. The following sections provide a comprehensive rationale for our model selection and confirm their suitability for a direct and understandable comparison.

Justification behind the Choice of Cu Nanowire on ZnO. The rationale for choosing the Cu nanowire model instead of Cu nanoparticles is that our ability to work with larger model systems is limited by the size of the DFT

https://doi.org/10.1021/acs.jpcc.4c08821
J. Phys. Chem. C 2025, 129, 5860−5867

calculations that we use. This precludes efficient calculations of supported copper clusters with more than 50 atoms. The result would be models of copper particles in the nm or sub-nm zone, similar to what has been seen for Au and Pt particles, where quantum size effects are expected because the metallic s and p states are still relatively localized, instead of forming a broad sp-band.[54,56,57]

In the previous research, it has for example been shown that metallic Cu clusters exhibiting a size of 55 atoms show a localized sp-band, whereas a Cu-nanowire shows a broad sp-band similar to what is shown by the Cu (111) infinite model system.[52] Computational nanowire models are therefore not subject to quantum size effects due to their quasi-one-dimensional periodicity. Hence, unlike subnanometer metal clusters, these nanowires might potentially represent much bigger Cu nanoparticles (with a diameter of 2 nm or more, as observed in the experimental investigations).

The Cu-NW model's capacity to represent essential surface facets, particularly stepped facets vital for catalytic reactions, is another notable advantage. Figure 1A distinctly depicts the Cu nanowire situated on the ZnO (10−10) surface (denoted Cu/ZnO). The side view (left) and top view (right) emphasize the distinct surface facets shown on the nanowire, encompassing the (100), (111), and (211) planes. The significance of these facets lies in the fact that stepped facets with low-coordination sites, like the (211) plane, situated near the interface region, frequently demonstrate increased catalytic activity owing to their capacity to stabilize reaction intermediates thus potentially promoting important reaction pathways.[58] By choosing the Cu nanowire model, we can accurately capture essential surface characteristics, especially at contact with the oxide support, facilitating a more precise depiction of catalytic processes at the metal−metal oxide interface.

Justification behind the Choice of ZnO Nanowire on Cu. In order to have a fair comparison between Cu/ZnO and its inverse model, we created an analogous model where a ZnO nanowire is placed on a Cu (111) surface, denoted as ZnO/Cu (Figure 1B). This model allows us to probe the interaction of ZnO and also to investigate to what extent reduced ZnO ($Zn^{\delta+}$) alters the reaction mechanisms, while we will not investigate the surface alloy formation of CuZn in this study. This inverted catalyst reflects the geometry of the Cu nanowire supported on a ZnO (10−10) surface, as depicted in Figure 1A. We therefore have two complementary models (Cu/ZnO and ZnO/Cu) illustrating metal/metal oxide as well as inverse metal oxide/metal interfaces.

CO_2 and CO Hydrogenation Reaction Intermediates. Using these two model catalysts we employed DFT calculations to compute the stability of all intermediates occurring in the conversion of both CO_2 and CO to methanol, the mechanistic details of which are well-established in the literature.[39,59] Intermediates in the CO_2 hydrogenation involve formate (HCOO), formic acid (HCOOH), and hydroxymethylene (H_2COOH). The latter is assumed to break the C−O bond, thus yielding adsorbed formaldehyde (H_2CO) and hydroxyl (OH). Adsorbed H_2CO is then hydrogenated to methanol (CH_3OH) through the methoxy (CH_3O) intermediate. Surface OH is subsequently eliminated in the form of water. Note that H_2CO and H_3CO are intermediates in both CO and CO_2 hydrogenation. Below, we discuss the intermediates for both CO_2 and CO hydrogenation steps and analyze their stability on both types of interfaces.

Formate (HCOO). Formate is a crucial reaction intermediate in the hydrogenation of CO_2 to methanol, with numerous theoretical and experimental investigations hinting at the speciation and role of HCOO* on Cu surfaces.[60,61] Experimental data on HCOO* on Cu (111) indicate the presence of a single bidentate species.[62,63] For our calculations, we considered three possible adsorption sites, namely, the interface site (Figure 2A,D) between the nanowire and the

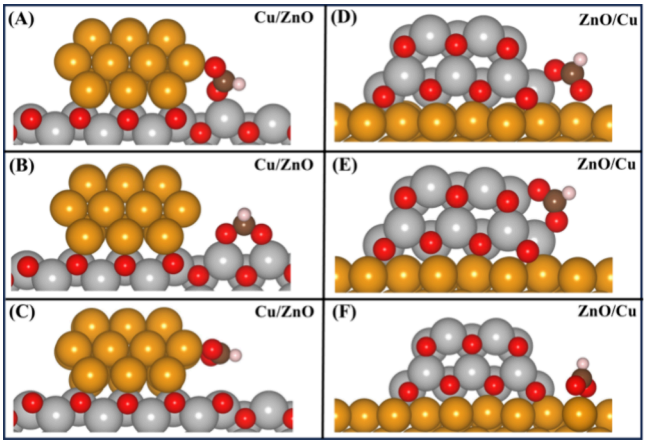

Figure 2. Adsorption of formate (HCOO) on the Cu/ZnO and ZnO/Cu configurations. Panels (A−C) illustrate the adsorption of formate on the Cu nanowire supported by the ZnO (10−10) surface. (A) Formate adsorbed at the interface site, (B) formate adsorbed at the ZnO surface site adjacent to the interface, and (C) formate adsorbed at the Cu surface site adjacent to the interface. Panels (D−F) depict the inverse configuration, featuring a ZnO nanowire positioned on the Cu (111) surface. (D) Formate adsorbed at the interface site, (E) formate adsorbed at the ZnO surface site adjacent to the interface, and (F) formate adsorbed at the Cu surface site adjacent to the interface. In all instances, the formate species bonds in a bidentate structure via both oxygen atoms.

support and the surface sites ZnO (Figure 2B,E) and Cu (Figure 2C,F) near the interface. As from Figure 2, it is seen that HCOO* binds through both oxygen atoms for both models. The Cu/ZnO interface exhibits optimal HCOO* adsorption (Figure 2A), with a binding energy of −1.44 eV (Table 1). Contrarily, the adsorption of formate on the nearby ZnO surface site (Figure 2B) is around −0.96 eV and that on the nearby Cu surface site (Figure 2C) is around −1.32 eV. On the other hand, the HCOO* at ZnO/Cu slightly favors the ZnO surface site (Figure 2E) with a binding energy of −1.45 eV (see Table 1) over the interface site (Figure 2D) with a binding energy of −1.19 eV and the nearby Cu surface site (Figure 2F) with a binding energy of −0.80 eV.

Bader charge analysis of the Zn and Cu species involved in HCOO binding (Table S1) shows that a slightly reduced Zn species at the interface of ZnO/Cu (Figure 2D,E) provides a suitable adsorption site for HCOO adsorption. Interestingly, we observe that the binding energy difference of HCOO* at the most favorable adsorption locations for both models (Figure 2A,E) is essentially negligible (approximately 0.01 eV) and that the overall charge transfer is almost the same (Table S2). This is particularly noteworthy, as it indicates that the performance of the interface region for either the catalyst or inverse catalyst exhibits no marked differences with respect to the HCOO* intermediate.

https://doi.org/10.1021/acs.jpcc.4c08821
J. Phys. Chem. C 2025, 129, 5860−5867

Table 1. Binding Energies of the Intermediates at the Most Favorable Adsorption Site for the Hydrogenation of CO/CO_2 to Methanol of Both Models[a]

intermediates	binding energy (eV): Cu/ZnO	binding energy (eV): ZnO/Cu
CO*	−0.68	−0.44
HCOO*	−1.44	−1.45
H_2COO*	−0.96	−0.60
HCOOH*	−1.17	−1.01
H_2COOH*	−0.89	−0.84
HCO*	−0.44	−0.30
HCO*_$O_{lattice}$	−1.23	−1.59
H_2CO*	−1.13	−0.98
H_2CO*_$O_{lattice}$	−1.48	−1.13
OH*	−1.37	−1.45
H_3CO*	−1.81	−1.70
H*	−0.03	−0.05

[a]The geometries are given in Figures 2A,E and 4 and Figures S1−S7 (see SI).

For each intermediate studied, as for HCOO, all three possible adsorption sites, the interface and the surface ZnO and Cu near the interface, were considered. However, since most of the intermediates spontaneously move to their most stable configuration during geometry optimization, we present only the most favorable structures in the following text.

Dioxymethylene vs Formic Acid (H_2COO vs HCOOH). Formate is the most stable intermediate in methanol synthesis on Cu, and its subsequent hydrogenation to methoxy (CH_3O) is commonly considered the step that dictates the reaction rate. Nonetheless, the creation of CH_3O from HCOO* necessitates the formation of two C−H bonds and the cleavage of one C−O bond. The simultaneous occurrence of these three bond formations and breaking events is improbable, leading one to anticipate a sequential mechanism via less stable surface intermediates. The stepwise hydrogenation process can be initiated at either the C or the O atom of the HCOO* species, resulting in the formation of dioxymethylene (H_2COO, as shown in Figure S1A,B) or formic acid (HCOOH, as depicted in Figure S1C,D), respectively. Similar to the case for HCOO*, H_2COO* binds to the surface with both the O atoms. The most stable binding mode for H_2COO on both nanowires (Cu/ZnO and ZnO/Cu) is at the interface (see SI, Figure S1(A) and (B)), with binding energy of −0.96 eV and −0.60 eV respectively (see Table 1). Our calculations revealed that compared to the H_2COO* intermediate, HCOOH* is the more stable entity. For both models Cu/ZnO and ZnO/Cu, HCOOH* binds favorably at the interface region with binding energies of −1.17 eV (Cu/ZnO) and −1.01 eV (ZnO/Cu), (see Table 1). Notably, the observed discrepancy in binding energies for both models is rather small.

Hydroxymethoxy (H_2COH). The generation of the H2COOH intermediate from HCOOH during the CO_2 hydrogenation to methanol constitutes the next step in the overall reaction process.[47] Figure S2 illustrates the binding of the H_2COOH* intermediate on both models. H_2COOH* binds with both of its oxygen centers to the Cu surface. It is seen that for both models H_2COOH* prefers to bind at the interface sites and the corresponding binding energies are −0.89 and −0.84 eV for Cu/ZnO and ZnO/Cu models, respectively (Figure S2A,B). Despite the small differences in binding energies, the most stable positions of H_2COOH* are analogous in both models.

Formaldehyde (H_2CO).* During the CO_2 hydrogenation process, the H_2COOH intermediate dissociates into formaldehyde (H_2CO) and hydroxy (OH) species. H_2CO* prefers to bind on the ZnO site near the interface region for both models. The binding energies are −1.13 and −0.98 eV for Cu/ZnO and ZnO/Cu models, respectively (see Table 1). We also tested the possibility of an oxygen-assisted conformation (H_2CO*_Olattice) and found that for both models this is energetically more favorable (−1.48 eV for Cu/ZnO and −1.13 eV for ZnO/Cu) (see Table 1) compared to the H_2CO*, confirming the importance of considering O-assisted intermediates. Figure S3 shows the binding positions of H_2CO* over both the models using normal (Figure S3A,B) as well as O-assisted conformation (Figure S3C,D).

Hydroxy (OH). In the stepwise hydrogenation process during CO_2 conversion, the hydroxy (OH) intermediate forms. Figure S4 illustrates the binding of OH* on both models. The binding energies are −1.37 and −1.45 eV, respectively, for Cu/ZnO and ZnO/Cu. As the direct interfacial site is not accessible due to limited space, it is seen that for Cu/ZnO, OH* prefers to bind at the stepped facet site (211) of Cu nanowire (see Figure S4A), whereas for ZnO/Cu, OH* binds at the interface site (see Figure S4B).

Methoxy (CH_3O).* The last intermediate for stepwise hydrogenation from CO_2 to CH_3OH is CH_3O*.[64,65] While the methoxy intermediate adsorbs strongly on both models, we find that the binding energy difference between the two models is only ∼0.11 eV (−1.81 eV Cu/ZnO vs −1.70 eV ZnO/Cu) (see Table 1 and Figure S5). From Figure S5A, it is seen that the methoxy intermediate binds to the (211) facet of the Cu/ZnO model, with the oxygen atom directly engaging with the Cu surface. Conversely, Figure S5 illustrates the binding of the methoxy intermediate to the ZnO/Cu model with the contact also facilitated by the oxygen atom. Despite the structural differences between methoxy binding to Cu/ZnO and ZnO/Cu, both models exhibit similar binding energies.

Free Energy Diagram for CO_2 Hydrogenation. Figure 3 illustrates the free energy diagram of the hydrogenation of CO_2

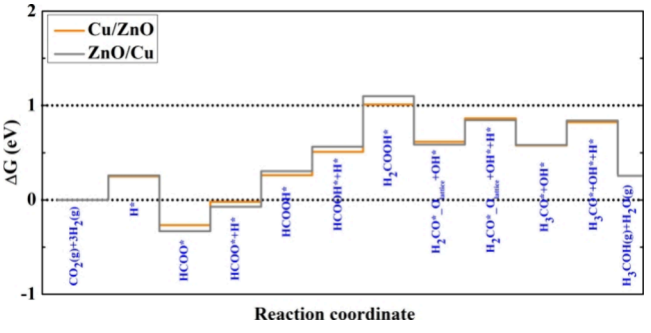

Figure 3. Calculated free energy diagram for CO_2 hydrogenation to methanol (temperature = 500 K and pressure = 1 bar) over Cu/ZnO (orange) and ZnO/Cu (gray) models.

to methanol using Cu/ZnO and ZnO/Cu. Interestingly, our results indicate that both models have fairly similar thermodynamics regarding the reaction mechanism with differences being less than 0.08 eV. The generation and stabilization of critical intermediates, including HCOO*, H_2COOH*, and H_3CO*, occur with negligible differences

https://doi.org/10.1021/acs.jpcc.4c08821
J. Phys. Chem. C 2025, 129, 5860−5867

between the two models. This indicates that the energetics of CO_2 hydrogenation are similar for Cu supported on ZnO and for ZnO being dispersed on copper surfaces. We note that this is very much in line with experiments comparing Cu/ZnO with ZnO-doped Cu/MgO catalysts for CO_2 hydrogenation, which both exhibit similar overall activity but also behavior in terms of activity when evaluated as a function of CO_2 in the synthesis gas.[66]

Carbon Monoxide (CO).* We systematically studied the binding of CO* on both models. From Figure S6, it can be seen that CO* prefers to bind on the copper sites for both models. In the Cu/ZnO model (Figure S6A), binding occurs at the Cu (211) edge with a binding energy of −0.68 eV and in the ZnO/Cu model (Figure S6B); binding also occurs at the Cu surface site with a binding energy of −0.44 eV. The differences in binding energies can be attributed to the fact that for Cu/ZnO, there exists a Cu (211) site, whereas for ZnO/Cu, the available site is the Cu (111) facet.

Formyl (HCO).* Formyl binds strongly to the interfaces on both Cu/ZnO and ZnO/Cu. In the case of Cu/ZnO, it binds on the (211) facet of Cu with (Figure 4A) a binding energy of −0.44 eV (see Table 1). For ZnO/Cu, the binding energy is −0.31 eV. Also, it is found that HCO* prefers to bind to the ZnO/Cu site in a bridging mode, with oxygen binding to ZnO and carbon binding to Cu (Figure 4B). One interesting observation is that the formyl intermediate can bind to an oxygen atom of ZnO thus forming a formate-like species with one of the oxygens being within the ZnO lattice (denoted HCO*_$O_{lattice}$) as also proposed by Jensen et al. albeit for MgO as the support.[67] These configurations are significantly more stable compared to the HCO* intermediate (Figure 4C,D), with adsorption energies of −1.23 and −1.67 eV for Cu/ZnO and ZnO/Cu, respectively. This shows that the oxygen-assisted pathway leading to the formation of a stable intermediate can play a pivotal role.

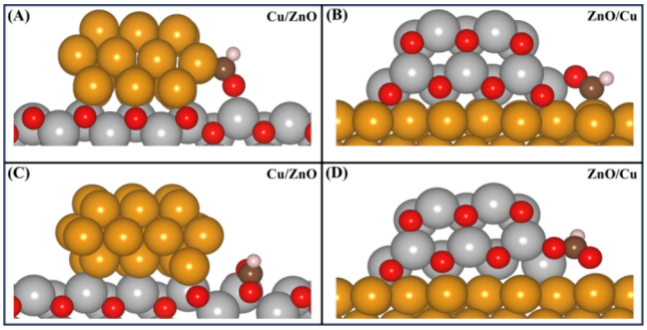

Figure 4. HCO* adsorption on the (A) Cu/ZnO and (B) ZnO/Cu models. Bottom panels show the HCO* adsorption through O-assisted mode on (C) Cu/ZnO and (D) ZnO/Cu models.

Free Energy Diagram for CO Hydrogenation. The free energy diagram in Figure 5 illustrates the CO hydrogenation process for both the Cu/ZnO and ZnO/Cu model at 500 K temperature and 1 bar pressure. The reaction mechanism is illustrated by depicting the changes in Gibbs free energy as carbon monoxide undergoes hydrogenation and transitions through various intermediates (CO*, HCO*, H_2CO*, and H_3CO*), leading to methanol formation. Both models display analogous free energy profiles but also exhibit differences. CO adsorption onto the catalyst surface is energetically uphill for both models at 500 K.

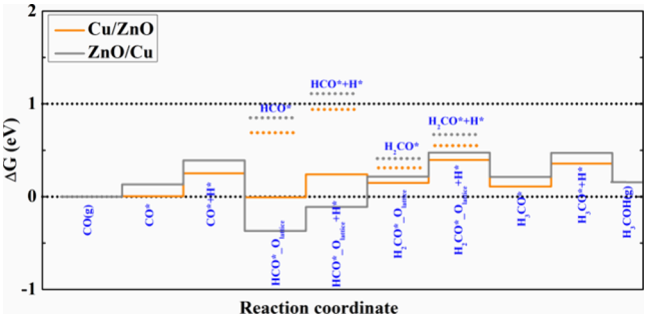

Figure 5. Calculated free energy diagram for hydrogenation of CO to methanol (temperature = 500 K, pressure = 1 bar) based on Cu/ZnO (orange) and ZnO/Cu (gray) models. Dotted lines represent less stable, nonoxygen-assisted HCO* and H_2CO* species.

The following hydrogenation of CO* to HCO* exhibits a minor free energy change for both models, with the ZnO/Cu model presenting marginally smaller binding energies (dashed lines). On the other hand, the more stable conformation, the oxygen-assisted HCO*_$O_{lattice}$ intermediate (solid line), shows a slightly larger difference between the two models. The HCO*_$O_{lattice}$ intermediate exhibits substantial stabilization in both models, attaining a minimum in free energy, indicating that this step is extremely advantageous and potentially a crucial intermediate in CO hydrogenation. The subsequent hydrogenation of HCO* to H_2CO* and ultimately to H_3CO* occurs with minimal free energy changes, suggesting that the transition among these intermediates is rather seamless for both models. The free energy diagram indicates that both models exhibit similar efficacy for CO hydrogenation, with the exception of the most stable HCO*_$O_{lattice}$ intermediate.

Vibrational Frequencies of the Intermediates. The computation of vibrational frequencies for CO_2 and CO hydrogenation intermediates is essential for comprehending catalytic mechanisms on the molecular scale. In addition, especially important is a comparison of characteristic vibrational modes of formate species, particularly in the C−H and C−O stretching regions, which can be directly probed using experimental techniques such as infrared (IR) or Raman spectroscopy. Here, we provide calculated frequencies for HCOO*, HCO*_$O_{lattice}$, and for HCO* species in Table 2 and for all intermediates in Table S3.

From Table 2, it can be seen that the vibration of the C−H stretching mode 2750−2800 cm^{-1} in normal HCO* species is shifted to 2900−3000 cm^{-1} for the HCO*_$O_{lattice}$, similar to HCOO*. On the other hand, the asymmetric O−C−O stretching mode shows some differences between

Table 2. Simulated Vibrational Frequencies of the HCOO* (Figure 2A,E), HCO*_$O_{lattice}$ (Figure 4C,D), and HCO* (Figure 4A,B) Intermediates for Both Models

vibrational mode	C−H	O−C−O(Cu) asymmetric	O−C−O(Cu) symmetric
HCOO* Cu/ZnO	2973	1525	1324
HCO*_$O_{lattice}$ Cu/ZnO	2995	1545	1242
HCO* Cu/ZnO	2756	1479	Nan
HCOO* ZnO/Cu	2966	1577	1322
HCO*_$O_{lattice}$ZnO/Cu	2913	1589	1227
HCO* ZnO/Cu	2808	1469	Nan

https://doi.org/10.1021/acs.jpcc.4c08821
J. Phys. Chem. C 2025, 129, 5860−5867

HCO*_$O_{lattice}$ and HCOO* species, but the symmetric O−C−O stretching is clearly different.

CONCLUSIONS

This study systematically investigates and compares the catalytic activity of metal-oxide interfaces in Cu/ZnO and its inverse counterpart, ZnO/Cu. We investigated intermediates in the reaction pathway for methanol production by concentrating on the hydrogenation reactions of both CO_2 and CO. Our comprehensive DFT-based computational investigation yielded significant insights into the binding energies and reaction energetics at the interface regions for both models. We investigated the essential function of oxygen-assisted routes in stabilizing intermediates, specifically HCO_O* and H_2CO_O*, and established that binding of intermediates to lattice oxygen of the ZnO component markedly improved the stability of these intermediates for both Cu/ZnO and ZnO/Cu. Due to the different stability of the oxygen atoms involved in Cu/ZnO and ZnO/Cu, there are distinct differences in the binding of the reaction intermediates, with the latter being stronger presumable due to the more active nature of lattice oxygen.

We believe that the principles of metal/metal oxide and metal oxide/metal interfaces are more generally applicable for oxide-supported and/or promoted transition metal catalysts and could aid in-depth understanding of surface geometries, electronic properties, and dynamic structural variations under reaction conditions. The observed influence of lattice oxygen-assisted routes on the stability of intermediates indicates that oxygen defects or the modification interface between the metal and metal oxide could lead to improved catalytic performance. While we have not investigated reaction-free energy barriers in the present study, it remains to be seen whether these will follow Brønsted−Evans−Polanyi relationships, thus scaling with the thermodynamics of the present study, or whether there are more intricate effects at the metal−metal oxide interface.

ASSOCIATED CONTENT

Supporting Information

The Supporting Information is available free of charge at https://pubs.acs.org/doi/10.1021/acs.jpcc.4c08821.

Cartesian coordinates for all optimized geometries (PDF)

Binding geometries of the intermediates; Gibbs free energy of the intermediates; parity plots for the CO_2 and CO hydrogenation intermediates; Bader charge analysis; vibrational frequencies of the intermediates; and thermochemistry data for the intermediates (PDF)

AUTHOR INFORMATION

Corresponding Author

Jelena Jelic − *Institute of Catalysis Research and Technology (IKFT), Karlsruhe Institute of Technology (KIT), EggensteinLeopoldshafen 76344, Germany;* orcid.org/0000-0002-2701-0765; Email: jelena.jelic@kit.edu

Authors

Chandra Chowdhury − *Institute of Catalysis Research and Technology (IKFT), Karlsruhe Institute of Technology (KIT), EggensteinLeopoldshafen 76344, Germany*

Felix Studt − *Institute of Catalysis Research and Technology (IKFT), Karlsruhe Institute of Technology (KIT), EggensteinLeopoldshafen 76344, Germany; Institute for Chemical Technology and Polymer Chemistry (ITCP), Karlsruhe Institute of Technology (KIT), Karlsruhe 76131, Germany;* orcid.org/0000-0001-6841-4232

Complete contact information is available at: https://pubs.acs.org/10.1021/acs.jpcc.4c08821

Author Contributions

The manuscript has written with the contributions from all the authors.

Funding

No competing financial interests have been declared.

Notes

The authors declare no competing financial interest.

ACKNOWLEDGMENTS

The authors acknowledge support by the state of Baden-Württemberg through bwHPC and the German Research Foundation (DFG) through grant no. INST 40/575-1 FUGG (JUSTUS 2 cluster, RVs bw17D011). The authors thank the Deutsche Forschungsgemeinschaft (DFG) for funding this work in the framework of the Priority Program SPP 2080 "Catalysts and reactors under dynamic conditions for energy storage and conversion" under the grant number STU 703/3-2. Financial support from the Helmholtz Association, Germany is also gratefully acknowledged.

REFERENCES

(1) Ro, I.; Resasco, J.; Christopher, P. Approaches for Understanding and Controlling Interfacial Effects in Oxide-Supported Metal Catalysts. *ACS Catal.* **2018**, *8* (8), 7368−87.

(2) Campbell, C. T. Electronic Perturbations. *Nat. Chem.* **2012**, *4* (8), 597−8.

(3) Laursen, S.; Linic, S. Oxidation Catalysis by Oxide-Supported Au Nanostructures: The Role of Supports and the Effect of External Conditions. *Phys. Rev. Lett.* **2006**, *97* (2), No. 026101.

(4) Jones, J.; Xiong, H.; DeLaRiva, A. T.; Peterson, E. J.; Pham, H.; Challa, S. R.; Qi, G.; Oh, S.; Wiebenga, M. H.; Pereira Hernández, X. I.; Wang, Y.; Datye, A. K. Thermally Stable Single-Atom Platinum-on-Ceria Catalysts via Atom Trapping. *Science* **2016**, *353* (6295), 150−154.

(5) Cargnello, M.; Doan-Nguyen, V. V.; Gordon, T. R.; Diaz, R. E.; Stach, E. A.; Gorte, R. J.; Fornasiero, P.; Murray, C. B. Control of Metal Nanocrystal Size Reveals Metal-Support Interface Role for Ceria Catalysts. *Science.* **2013**, *341* (6147), 771−3.

(6) Kudernatsch, W.; Peng, G.; Zeuthen, H.; Bai, Y.; Merte, L. R.; Lammich, L.; Besenbacher, F.; Mavrikakis, M.; Wendt, S. Direct Visualization of Catalytically Active Sites at the FeO−Pt (111) Interface. *ACS Nano* **2015**, *9* (8), 7804−14.

(7) Saavedra, J.; Doan, H. A.; Pursell, C. J.; Grabow, L. C.; Chandler, B. D. The Critical Role of Water at the Gold-Titania Interface in Catalytic CO Oxidation. *Science.* **2014**, *345* (6204), 1599−602.

(8) Chen, Z.; Mao, Y.; Chen, J.; Wang, H.; Li, Y.; Hu, P. Understanding the Dual Active Sites of the FeO/Pt (111) Interface and Reaction Kinetics: Density Functional Theory Study on Methanol Oxidation to Formaldehyde. *ACS Catal.* **2017**, *7* (7), 4281−90.

(9) Docherty, S. R.; Copéret, C. Deciphering Metal−Oxide and Metal−Metal Interplay via Surface Organometallic Chemistry: A Case Study with CO2 Hydrogenation to Methanol. *J. Am. Chem. Soc.* **2021**, *143* (18), 6767−80.

(10) Chen, Z.; Liu, Y.; Liu, C.; Zhang, J.; Chen, Y.; Hu, W.; Deng, Y. Engineering the Metal/Oxide Interface of Pd Nanowire@CuOx

Electrocatalysts for Efficient Alcohol Oxidation Reaction. *Small* **2020**, *16* (4), No. 1904964.
(11) Aranifard, S.; Ammal, S. C.; Heyden, A. On the Importance of Metal−Oxide Interface Sites for the Water−Gas Shift Reaction Over Pt/CeO2 Catalysts. *J. Catal.* **2014**, *309*, 314−24.
(12) Fernandez-Garcia, M.; Martinez-Arias, A.; Hanson, J. C.; Rodriguez, J. A. Nanostructured Oxides in Chemistry: Characterization and Properties. *Chem. Rev.* **2004**, *104* (9), 4063−104.
(13) Li, Y.; Zhang, Y.; Qian, K.; Huang, W. Metal−Support Interactions in Metal/Oxide Catalysts and Oxide−Metal Interactions in Oxide/Metal Inverse Catalysts. *ACS Catal.* **2022**, *12* (2), 1268−1287.
(14) Graciani, J.; Mudiyanselage, K.; Xu, F.; Baber, A. E.; Evans, J.; Senanayake, S. D.; Stacchiola, D. J.; Liu, P.; Hrbek, J.; Sanz, J. F.; Rodriguez, J. A. Highly Active Copper-Ceria and Copper-Ceria-Titania Catalysts for Methanol Synthesis from CO2. *Science* **2014**, *345* (6196), 546−550.
(15) Rodriguez, J. A.; Ma, S.; Liu, P.; Hrbek, J.; Evans, J.; Perez, M. Activity of CeOx and TiOx Nanoparticles Grown on Au (111) in the Water-Gas Shift Reaction. *Science* **2007**, *318* (5857), 1757−1760.
(16) Pan, Q.; Weng, X.; Chen, M.; Giordano, L.; Pacchioni, G.; Noguera, C.; Goniakowski, J.; Shaikhutdinov, S.; Freund, H. J. Enhanced CO Oxidation on the Oxide/Metal Interface: From Ultrahigh Vacuum to Near-Atmospheric Pressures. *ChemCatChem.* **2015**, *7* (17), 2620−2627.
(17) Freund, H. J. Metal-Supported Ultrathin Oxide Film Systems as Designable Catalysts and Catalyst Supports. *Surf. Sci.* **2007**, *601* (6), 1438−1442.
(18) Fu, Q.; Yang, F.; Bao, X. Interface-Confined Oxide Nanostructures for Catalytic Oxidation Reactions. *Acc. Chem. Res.* **2013**, *46* (8), 1692−1701.
(19) Li, Y.; Li, Z.; Hu, J.; Huang, W. Electronic Oxide-Metal Strong Interactions (EOMSI) Localized at CeOx-Ag Interface. *J. Phys. Chem. Lett.* **2024**, *15* (34), 8682−8688.
(20) Qian, K.; Duan, H.; Li, Y.; Huang, W. Electronic Oxide−Metal Strong Interaction (EOMSI). *Chem. - Eur. J.* **2020**, *26* (60), 13538−13542.
(21) Ren, M.; Qian, K.; Huang, W. Electronic Metal-Support Interaction-Modified Structures and Catalytic Activity of CeOx Overlayers in CeOx/Ag Inverse Catalysts. *Chem. - Eur. J.* **2019**, *25* (70), 15978−15982.
(22) Chang, S.; Ruan, S.; Wu, E.; Huang, W. CeO2 Thickness-dependent SERS and Catalytic Properties of CeO2-on-Ag Particles Synthesized by O2-Assisted Hydrothermal Method. *J. Phys. Chem. C* **2014**, *118* (33), 19238−19245.
(23) Rodriguez, J. A.; Liu, P.; Graciani, J.; Senanayake, S. D.; Grinter, D. C.; Stacchiola, D.; Hrbek, J.; Fernández-Sanz, J. Inverse Oxide/Metal Catalysts in Fundamental Studies and Practical Applications: A Perspective of Recent Developments. *J. Phys. Chem. Lett.* **2016**, *7* (13), 2627−2639.
(24) Dalebout, R.; Visser, N. L.; Pompe, C. L.; de Jong, K. P.; de Jongh, P. E. 2020. Interplay Between Carbon Dioxide Enrichment and Zinc Oxide Promotion of Copper Catalysts in Methanol Synthesis. *J. Catal.* **2020**, *392*, 150−158.
(25) Kattel, S.; Ramírez, P. J.; Chen, J. G.; Rodriguez, J. A.; Liu, P. Active sites for CO2 Hydrogenation to Methanol on Cu/ZnO Catalysts. *Science* **2017**, *355* (6331), 1296−1299.
(26) Pandit, L.; Boubnov, A.; Behrendt, G.; Mockenhaupt, B.; Chowdhury, C.; Jelic, J.; Hansen, A.; Saraçi, E.; Ras, E.; Behrens, M.; Studt, F.; Grunwaldt, J. Unravelling the Zn-Cu Interaction During Activation of a Zn-promoted Cu/MgO Model Methanol Catalyst. *ChemCatChem* **2021**, *13* (19), 4120−4132.
(27) Yang, S. C.; Pang, S. H.; Sulmonetti, T. P.; Su, W. N.; Lee, J. F.; Hwang, B. J.; Jones, C. W. Synergy Between Ceria Oxygen Vacancies and Cu Nanoparticles Facilitates the Catalytic Conversion of CO2 to CO under Mild Conditions. *ACS Catal.* **2018**, *8* (12), 12056−12066.
(28) Wang, Y.; Chan, Y. S.; Zhang, R.; Yan, B. Insights into the Contribution of Oxygen Vacancies on CO2 Activation for Dry Reforming of Methane over Ceria-Based Solid Solutions. *Chem. Eng. J.* **2024**, *481*, No. 148360.
(29) Deng, Z.; Ji, J.; Xing, M.; Zhang, J. The Role of Oxygen Defects in Metal Oxides for CO2 Reduction. *Nanoscale Adv.* **2020**, *2* (11), 4986−4995.
(30) Behrens, M.; Studt, F.; Kasatkin, I.; Kühl, S.; Hävecker, M.; Abild-Pedersen, F.; Zander, S.; Girgsdies, F.; Kurr, P.; Kniep, B. L.; Tovar, M.; Fischer, R. W.; Nørskov, J. K.; Schlögl, R. The Active Site of Methanol Synthesis over Cu/ZnO/Al2O3 Industrial Catalysts. *Science* **2012**, *336* (6083), 893−897.
(31) Choi, Y.; Futagami, K.; Fujitani, T.; Nakamura, J. The Difference in the Active Sites for CO2 and CO Hydrogenations on Cu/ZnO-Based Methanol Synthesis Catalysts. *Catal. Lett.* **2001**, *73*, 27−31.
(32) Kuld, S.; Thorhauge, M.; Falsig, H.; Elkjær, C. F.; Helveg, S.; Chorkendorff, I.; Sehested, J. Quantifying the Promotion of Cu Catalysts by ZnO for Methanol Synthesis. *Science* **2016**, *352* (6288), 969−974.
(33) Li, J.; Wang, D.; Xiong, W.; Ding, J.; Huang, W. Interfacial Site Density Engineering of ZnO/Cu Cube Inverse Catalysts for CO2 Hydrogenation Reactions. *ACS Catal.* **2024**, *14* (23), 17413−17420.
(34) Kordus, D.; Jelic, J.; Lopez Luna, M.; Divins, N. J.; Timoshenko, J.; Chee, S. W.; Rettenmaier, C.; Kröhnert, J.; Kühl, S.; Trunschke, A.; Schlögl, R.; Studt, F.; Roldan Cuenya, B. Shape-Dependent CO2 Hydrogenation to Methanol over Cu2O Nanocubes Supported on ZnO. *J. Am. Chem. Soc.* **2023**, *145* (5), 3016−3030.
(35) Xiong, W.; Ding, J.; Wang, D.; Huang, W. Cu Facet-Dependent Elementary Surface Reaction Kinetics of CO2 Hydrogenation to Methanol Catalyzed by ZrO2/Cu Inverse Catalysts. *J. Phys. Chem. Lett.* **2023**, *14* (32), 7229−7234.
(36) Kordus, D.; Widrinna, S.; Timoshenko, J.; Lopez Luna, M.; Rettenmaier, C.; Chee, S. W.; Ortega, E.; Karslioglu, O.; Kühl, S.; Roldan Cuenya, B. Enhanced Methanol Synthesis from CO2 Hydrogenation Achieved by Tuning the Cu−ZnO Interaction in ZnO/Cu2O Nanocube Catalysts Supported on ZrO2 and SiO2. *J. Am. Chem. Soc.* **2024**, *146* (12), 8677−8687.
(37) Zhang, Z.; Wang, S. S.; Song, R.; Cao, T.; Luo, L.; Chen, X.; Gao, Y.; Lu, J.; Li, W. X.; Huang, W. The Most Active Cu Facet for Low-Temperature Water Gas Shift Reaction. *Nat. Commun.* **2017**, *8* (1), 488.
(38) Zhang, Z.; Chen, X.; Kang, J.; Yu, Z.; Tian, J.; Gong, Z.; Jia, A.; You, R.; Qian, K.; He, S.; Teng, B.; Cui, Y.; Wang, Y.; Zhang, W.; Huang, W. The Active Sites of Cu−ZnO Catalysts for Water Gas Shift and CO Hydrogenation Reactions. *Nat. Commun.* **2021**, *12* (1), 4331.
(39) Studt, F.; Behrens, M.; Kunkes, E. L.; Thomas, N.; Zander, S.; Tarasov, A.; Schumann, J.; Frei, E.; Varley, J. B.; Abild-Pedersen, F.; Nørskov, J. K.; Schlögl, R. The Mechanism of CO and CO2 Hydrogenation to Methanol over Cu-Based Catalysts. *ChemCatChem* **2015**, *7* (7), 1105−1111.
(40) Kresse, G.; Furthmüller, J. Efficient Iterative Schemes for Ab Initio Total-Energy Calculations Using a Plane-Wave Basis Set. *Phys. Rev. B* **1996**, *54* (16), 11169.
(41) Kresse, G.; Furthmüller, J. Efficiency of Ab-Initio Total Energy Calculations for Metals and Semiconductors Using a Plane-Wave Basis Set. *Comput. Mater. Sci.* **1996**, *6* (1), 15−50.
(42) Bahn, S. R.; Jacobsen, K. W. An Object-Oriented Scripting Interface to a Legacy Electronic Structure Code. *Comp. Sci. Eng.* **2002**, *4* (3), 56−66.
(43) Blöchl, P. E. Projector Augmented-Wave Method. *Phys. Rev. B* **1994**, *50* (24), 17953.
(44) Kresse, G.; Joubert, D. From Ultrasoft Pseudopotentials to the Projector Augmented-Wave Method. *Phys. Rev. B* **1999**, *59* (3), 1758.
(45) Wellendorff, J.; Lundgaard, K. T.; Møgelhøj, A.; Petzold, V.; Landis, D. D.; Nørskov, J. K.; Bligaard, T.; Jacobsen, K. W. Density Functionals for Surface Science: Exchange-Correlation Model Development with Bayesian Error Estimation. *Phys. Rev. B* **2012**, *85* (23), No. 235149.
(46) Mallikarjun Sharada, S.; Bligaard, T.; Luntz, A. C.; Kroes, G. J.; Nørskov, J. K. SBH10: A Benchmark Database of Barrier Heights on

https://doi.org/10.1021/acs.jpcc.4c08821
J. Phys. Chem. C 2025, 129, 5860−5867

Transition Metal Surfaces. *J. Phys. Chem. C* **2017**, *121* (36), 19807−19815.
(47) Studt, F.; Abild-Pedersen, F.; Varley, J. B.; Nørskov, J. K. CO and CO2 Hydrogenation to Methanol Calculated Using the BEEF-vdW Functional. *Catal. Lett.* **2013**, *143*, 71−73.
(48) Wellendorff, J.; Silbaugh, T. L.; Garcia-Pintos, D.; Nørskov, J. K.; Bligaard, T.; Studt, F.; Campbell, C. T. A Benchmark Database for Adsorption Bond Energies to Transition Metal Surfaces and Comparison to Selected DFT Functionals. *Surf. Sci.* **2015**, *640*, 36−44.
(49) Studt, F.; Behrens, M.; Abild-Pedersen, F. Energetics of the Water−Gas-Shift Reaction on the Active Sites of the Industrially Used Cu/ZnO/Al2O3 Catalyst. *Catal. Lett.* **2014**, *144*, 1973−1977.
(50) Zhao, Z. J.; Li, Z.; Cui, Y.; Zhu, H.; Schneider, W. F.; Delgass, W. N.; Ribeiro, F.; Greeley, J. Importance of Metal-Oxide Interfaces in Heterogeneous Catalysis: A Combined DFT, Microkinetic, and Experimental Study of Water-Gas Shift on Au/MgO. *J. Catal.* **2017**, *345*, 157−169.
(51) Whittaker, T.; Kumar, K. S.; Peterson, C.; Pollock, M. N.; Grabow, L. C.; Chandler, B. D. H2 Oxidation Over Supported Au Nanoparticle Catalysts: Evidence for Heterolytic H2 Activation at the Metal−Support Interface. *J. Am. Chem. Soc.* **2018**, *140* (48), 16469−16487.
(52) Polierer, S.; Jelic, J.; Pitter, S.; Studt, F. On the Reactivity of the Cu/ZrO2 System for the Hydrogenation of CO2 to Methanol: A Density Functional Theory Study. *J. Phys. Chem. C* **2019**, *123* (44), 26904−26911.
(53) Hakimioun, A. H.; Vandegehuchte, B. D.; Curulla-Ferre, D.; Kaźmierczak, K.; Plessow, P. N.; Studt, F. Metal−Support Interactions in Heterogeneous Catalysis: DFT Calculations on the Interaction of Copper Nanoparticles with Magnesium Oxide. *ACS Omega* **2023**, *8* (11), 10591−10599.
(54) Hakimioun, A. H.; Dietze, E. M.; Vandegehuchte, B. D.; Curulla-Ferre, D.; Joos, L.; Plessow, P. N.; Studt, F. Theoretical Investigation of the Size Effect on the Oxygen Adsorption Energy of Coinage Metal Nanoparticles. *Catal. Lett.* **2021**, *151*, 3165−3169.
(55) Monkhorst, H. J.; Pack, J. D. Special Points for Brillouin-Zone Integrations. *Phys. Rev. B* **1976**, *13* (12), 5188.
(56) Kleis, J.; Greeley, J.; Romero, N. A.; Morozov, V. A.; Falsig, H.; Larsen, A. H.; Lu, J.; Mortensen, J. J.; Dułak, M.; Thygesen, K. S.; Nørskov, J. K.; Jacobsen, K. W. Finite Size Effects in Chemical Bonding: From Small Clusters to Solids. *Catal. Lett.* **2011**, *141*, 1067−1071.
(57) Li, L.; Larsen, A. H.; Romero, N. A.; Morozov, V. A.; Glinsvad, C.; Abild-Pedersen, F.; Greeley, J.; Jacobsen, K. W.; Nørskov, J. K. Investigation of Catalytic Finite-Size-Effects of Platinum Metal Clusters. *J. Phys. Chem. Lett.* **2013**, *4* (1), 222−226.
(58) Füchsel, G.; Cao, K.; Er, S.; Smeets, E. W.; Kleyn, A. W.; Juurlink, L. B.; Kroes, G. J. Anomalous Dependence of the Reactivity on the Presence of Steps: Dissociation of D2 on Cu (211). *J. Phys. Chem. Lett.* **2018**, *9* (1), 170−175.
(59) Grabow, L. C.; Mavrikakis, M. Mechanism of Methanol Synthesis on Cu Through CO2 and CO Hydrogenation. *ACS Catal.* **2011**, *1* (4), 365−384.
(60) Bowker, M.; Hadden, R. A.; Houghton, H.; Hyland, J. N. K.; Waugh, K. C. The Mechanism of Methanol Synthesis on Copper/Zinc Oxide/Alumina Catalysts. *J. Catal.* **1988**, *109* (2), 263−273.
(61) Walker, A. P.; Lambert, R. M.; Nix, R. M.; Jennings, J. R. Methanol Synthesis over Catalysts Derived from CeCu2: Transient Studies with Isotopically Labelled Reactants. *J. Catal.* **1992**, *138* (2), 694−713.
(62) Hayden, B. E.; Prince, K.; Woodruff, D. P.; Bradshaw, A. M. An IRAS Study of Formic Acid and Surface Formate Adsorbed on Cu (110). *Surf. Sci.* **1983**, *133* (2−3), 589−604.
(63) Sotiropoulos, A.; Milligan, P. K.; Cowie, B. C. C.; Kadodwala, M. A Structural Study of Formate on Cu (111). *Surf. Sci.* **2000**, *444* (1−3), 52−60.
(64) Edwards, J. F.; Schrader, G. L. Infrared Spectroscopy of Copper/Zinc Oxide Catalysts for the Water-Gas Shift Reaction and Methanol Synthesis. *J. Phys. Chem.* **1984**, *88* (23), 5620−5624.
(65) Weigel, J.; Fröhlich, C.; Baiker, A.; Wokaun, A. Vibrational Spectroscopic Study of IB Metal/Zirconia Catalysts for the Synthesis of Methanol. *Appl. Catal. Gen.* **1996**, *140* (1), 29−45.
(66) Behrendt, G.; Mockenhaupt, B.; Prinz, N.; Zobel, M.; Ras, E. J.; Behrens, M. CO Hydrogenation to Methanol over Cu/MgO Catalysts and Their Synthesis from Amorphous Magnesian Georgeite Precursors. *ChemCatChem* **2022**, *14* (17), No. e202200299.
(67) Nielsen, N. D.; Thrane, J.; Jensen, A. D.; Christensen, J. M. Bifunctional Synergy in CO Hydrogenation to Methanol with Supported Cu. *Catal. Lett.* **2020**, *150*, 1427−1433.

https://doi.org/10.1021/acs.jpcc.4c08821
J. Phys. Chem. C 2025, 129, 5860−5867